23rd ABCM International Congress of Mechanical Engineering
December 6-11, 2015, Rio de Janeiro, RJ, Brazil

Secondary instability analysis of 3D laminar separation bubbles based on cross-plane WKB approximation

Elmer M. Gennaro
UNESP - Universidade Estadual Paulista, Campus São João da Boa Vista, São João da Boa Vista-SP, 13874-149, Brazil.
elmer.gennaro@sjbv.unesp.br

Daniel Rodríguez
Departamento de Engenharia Mecânica, Pontifícia Universidade Católica do Rio de Janeiro, Rio de Janeiro-RJ, 22453-900, Brazil.
danielrodalv84@gmail.com

Leandro Franco de Souza
Institute of Mathematical and Computer Sciences, University of São Paulo, São Carlos-SP, 13566-590, Brazil.
lefraso@icmc.usp.br

Abstract. *Laminar flow separation and the formation of closed separation bubbles is a problem of primary technological significance due to its strong relation with the aerodynamic properties of lifting surfaces operating at high angles-of-attack. The behavior of these laminar separation bubbles (LSB) is believed to be dominated by hydrodynamic instability processes. The present research builds upon the idea put forward by U. Dallmann in the late 80s, that a global instability mechanism may exist acting on two-dimensional recirculating flows, that under an infinitesimally weak perturbation originates a fully three-dimensional flow. In our previous research, we demonstrated that this instability is recovered as a 3D eigenmode of the linearized Navier-Stokes equations, and proposed a weakly nonlinear expansion of the center manifold to study the nature of the bifurcation associated with the primary 3D eigenmode. In this paper, we study the secondary instability of the fully 3D bifurcated flow by means of a novel technique that applies the weakly non-parallel (WKB) approximation to cross-stream planes. The results obtained show that the self-excited 3D global instability of LSB also has the potential of triggering a secondary instability mechanism that originates the flow unsteadiness.*

Keywords:*boundary layer, separated flow, global instability*

1. INTRODUCTION

The separation of the laminar boundary layer under an adverse pressure gradient and its subsequent turbulent reattachment, forming what is known as a laminar separation bubble, is a technological problem of primary technological significance with applications in aircraft wings, turbines blades and wind turbines. Despite extensive studies spanning the last 70 years, many questions related to the appearance, structure and instability properties of laminar separation bubbles still remain open. One of the most fundamental aspects that incidentally has received relatively less attention concerns the instability processes acting on separation bubbles in the absence of incoming disturbances or externally-imposed forcing, as well as the series of flow bifurcations that spontaneously transform a nominally two-dimensional and steady separation bubble into an unsteady and three-dimensional transitional one. The dominance of inflectional instability in configurations in which external disturbances are present in the flow has been widely documented (e.g. Dovgal *et al.* (1994), and the ability to characterize this instability by means of simple analysis based on the parallel-flow approach has precluded an earlier exploration of the *unforced* scenario. However, the absence of external excitation neglects the amplifier behavior altogether and then only self-excited global instabilities have the potential of initiating the transition process.

Allen and Riley (1995) and Hammond and Redekopp (1998) applied a weakly non-parallel stability analysis (Huerre and Monkewitz (1990)) to different two-dimensional models of laminar separation bubbles, with the aim of clarifying if a global instability mechanism associated with the existence of regions of absolute instability of disturbance waves. The former did not found absolutely unstable local eigenmodes, while the second concluded that separation bubbles with a minimum peak recirculation $U_{rev} \sim 25\%$ of the external flow were required for global oscillations to appear. Subsequent analyses by Alam and Sandham (2000) and Rist and Maucher (2002) agreed on a lower value of $u_{rev} \sim 15-20\%$. On the other hand, Theofilis *et al.* (2000) performed a stability analysis considering three-dimensional modal disturbances, assumed to be periodic in the spanwise direction and with arbitrary shape on the other two spatial directions and discovered one self-excited and stationary eigenmode. The conjectures put forward by Dallmann (Dallmann and Schewe (1987); Theofilis *et al.* (2000)) on the topological changes exerted by the three-dimensional eigenmode were studied by Rodríguez

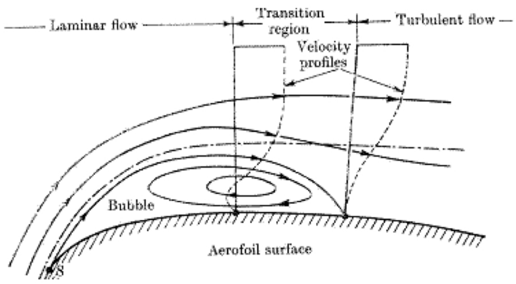

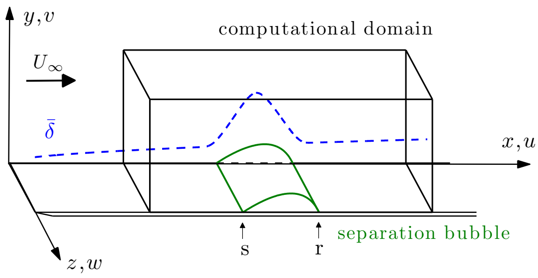

Figure 1. Left: Time average structure of the short leading-edge laminar separation bubble (from Horton (1969)). Right: Model configuration and computational domain.

and Theofilis (2010), who related them to the appearance of cellular patterns observed experimentally.

Rodríguez *et al.* (2013) study the competence of the two self-excited instability mechanisms, namely the global oscillator that transforms a steady two-dimensional bubble into an unsteady one, and the global eigenmode, associated to a centrifugal instability, that gives rise to a steady three-dimensionalization, in order to ascertain which of the two possible mechanisms should be expected to dominate. It was demonstrated that the three-dimensional global instability eigenmode becomes active for laminar separation bubbles that are significantly weaker (with a reversed-flow magnitude $u_{rev} \sim 7 - 8\%$) than that required for the onset of self-sustained two-dimensional oscillations. The implications of this finding, namely that unforced separation bubbles are prone to become three-dimensional as an effect of an intrinsic primary instability, were further studied in Rodríguez and Gennaro (2014). A weakly nonlinear expansion was presented, concluding that the primary instability is associated with an supercritical pitchfork bifurcation and that separation bubbles at supercritical conditions evolve into steady three-dimensional bubbles.

The secondary instability of the three-dimensional unforced LSBs resulting from the amplification of the centrifugal instability is addressed in this work. The framework for the study of global oscillators based on a weakly non-parallel approximation introduced by Huerre and Monkewitz (1990) and Chomaz *et al.* (1991) is extended here to three-dimensional flows by considering *local* analyses based on cross-stream sections. For the problem at hand, this methodology is shown to recover accurately results of an analysis based on fully three-dimensional eigenmodes, at a small fraction of the computational cost. Present results show that the three-dimensionalization of the unforced separation bubbles has the potential of triggering a secondary instability that results into fully three-dimensional and unsteady transitional flow.

The rest of the paper is organized as follows. Section 2 briefly outlines the main aspects of our previous research that are relevant for the present one. Section 3 is devoted to the secondary instability analysis: Section 3.1 describes the theoretical basis of the linear stability analysis for three-dimensional base states proposed herein, while Section 3.2 summarizes the numerical methods employed. The results are presented in Section 3.3. A discussion of the results closes the paper.

2. PREVIOUS RELATED WORK

2.1 A MODEL OF LEADING-EDGE LAMINAR SEPARATION BUBBLES

A flat-plate boundary-layer flow under an adverse pressure gradient is considered here as a model configuration for the leading-edge laminar separation bubble on a thin aerofoil when pitched up to a high enough angle of attack. The main assumption involved is that the curvature effects only play an role through the generation of the inviscid (external) flow deceleration. This model configuration has been used extensively in the literature (e.g. Dovgal *et al.* (1994); Alam and Sandham (2000); Rist and Maucher (2002)). The geometry along with the coordinate system is shown in figure 1.

We use an inverse-formulation of the non-similar, two-dimensional boundary-layer equations to compute a family of base laminar separation bubbles. In this formulation, a distribution of the boundary-layer displacement thickness $\bar{\delta}$ analogous to that of Carter (1975) is imposed and the corresponding external, inviscid flow is recovered as part of the solution; the distribution of displacement thickness is shown schematically in figure 1 (right). The Reynher and Flügge-Lotz approximation, that neglects the streamwise convective term when reversed flow exists, is invoked to allow for a downstream integration of the equations. The present methodology has been shown to recover realistic laminar separation bubbles, in good agreement with those obtained by direct numerical simulations, when a physically sensible distribution of displacement thickness is imposed (Rodríguez (2010)).

A series of laminar separation bubbles are constructed by varying the parameters in the analytical function defining the $\bar{\delta}(x)$ distribution. The displacement thickness is expressed in transformed boundary-layer variables so that for zero-pressure gradient (ZPG) the Blasius solution $\bar{\delta}_B = 1.7208...$ is imposed. External-flow deceleration corresponding to adverse-pressure gradients (APG) increases of the boundary-layer thickness $\bar{\delta} > \bar{\delta}_B$. The analytical function used to generate the separation bubbles, that can be found in Rodríguez and Theofilis (2010), defines a ZPG boundary-layer except of a bounded streamwise region in which $\bar{\delta}$ is increased up to a maximum value $\bar{\delta}_{max}$, then decreased back to $\bar{\delta}_B$. In the cases in which the imposed deceleration of the external flow is strong enough, a laminar separation bubble is formed. The three parameters defining the separation bubble are the streamwise locations where the deceleration begins and ends, respectively x_1 and x_2, and the maximum value of transformed displacement thickness $\bar{\delta}_{max}$ that is attained.

In the present paper, we consider a subset of the separation bubbles studied in Rodríguez *et al.* (2013) (denominated by letter L therein), where further details on the flow construction are given. The model separation bubbles considered herein have fixed x_1 and x_2, so the external flow deceleration has equal streamwise extent for all bubbles. $\bar{\delta}_{max}$ is varied, thus generating separation bubbles of different sizes and peak reversed flows $u_{0,rev}$ or recirculation, defined as the ratio between the maximum backflow within the bubble and the external flow velocity. The velocity fields obtained in this manner are transformed from the boundary-layer variables to physical ones and then scaled with the dimensional displacement thickness at a reference streamwise coordinate upstream of the APG, corresponding to a Reynolds number based on this displacement thickness of $Re = 450$, and a Reynolds number based on the separation bubble streamwise extent of approximately $Re_L = 49500$. The maximum peak reversed flow attained is $u_{0,rev} \approx 12\%$. The flowfields corresponding to the base separation bubbles discussed here will be referred to as $\bar{\mathbf{q}} = [\bar{u}(x,y)\ \bar{v}(x,y)]^T$.

2.2 PRIMARY INSTABILITY OF UNFORCED SEPARATION BUBBLES

The model separation bubbles discussed in the previous section are accurate solutions of the boundary-layer equations at high Reynolds numbers, and consequently are good approximations of the Navier-Stokes equations (the peak residual was found to be $\sim 3\%$). These base separation bubbles are two-dimensional and steady by construction; in those cases in which the flowfield is intrinsically unstable and would evolve towards a three-dimensional and/or unsteady flow, the responsible mechanism can be identified by means of linear instability analyses. Rodríguez *et al.* (2013) studied two possible self-excited instability mechanisms, i.e. instability modes that grow and have to potential of changing the flow conditions even in the absence of external forcing. Two mechanisms were analyzed: a flow oscillator originated by the existence of compact spatial regions of absolute instability of disturbance waves and a three-dimensional global eigenmode corresponding to a centrifugal instability. The former was found to be stable for all the bubbles analyzed, a finding in line with similar studies in the literate (Alam and Sandham (2000); Rist and Maucher (2002)) agreeing that a peak reversed flow of at least 16 % is required for this kind of instability to set in. The second mechanism was found to become active at peak reversed flows as low as $u_{0,rev} \sim 6 - 7\%$.

This centrifugal instability was recovered as an unstable eigenmode of the "global" eigenmode stability analysis resulting from assuming the perturbation form $\mathbf{q}' = \hat{\mathbf{q}}(x,y)\exp[\mathrm{i}(\beta z - \omega t)] + c.c.$ (with $c.c.$ standing for complex conjugate). In this framework, β is a real wavenumber on the spanwise direction, $\omega = \omega_r + \mathrm{i}\omega_i$ is a complex number with ω_r being a circular frequency and ω_i a temporal growth rate, and the shape functions $\hat{\mathbf{q}}(x,y)$ are two dimensional eigenfunctions comprising three velocity components and pressure: $\hat{\mathbf{q}} = [\hat{u}\ \hat{v}\ \hat{w}\ \hat{p}]^T$. The unstable eigenmode is characterized by the three following aspects: (i) the dominance of a finite spanwise wavenumber β, rendering the instability three-dimensional; (ii) the eigenmode is stationary ($\omega_r = 0$) for the range of unstable wavenumbers and (iii) it becomes unstable for peak reversed flows well below those required for absolute inflectional instability of local velocity profiles. The neutral curve for the three-dimensional eigenmode as a function of the peak recirculation $u_{0,rev}$ and spanwise wavenumber β is shown in figure 2 (a). Critical conditions were found to correspond to $\beta_c = 0.166$, and $u_{0,rev} \approx 7.1\%$.

The findings in Rodríguez *et al.* (2013) demonstrate that the transition scenario for unforced laminar separation bubbles commonly assumed in the literature, in which a self-excited inflectional gives rise to unsteadiness and then the three-dimensionality follows from a secondary instability, is not necessarily true or representative of all separation bubbles.

2.3 NONLINEAR SATURATION OF PRIMARY INSTABILITY

In view of the findings previously discussed, the question arises on the nature of the transition process initiated by linear growth of the three-dimensional eigenmode when disturbance amplitudes become finite and nonlinearity becomes important. With this aim, a weakly nonlinear (WNL) expansion of the Navier-Stokes equations is proposed to describe the bifurcated three-dimensional flow at finite disturbance amplitudes, for base separation bubbles close to the critical conditions. Details on the weakly nonlinear expansion can be found in Rodríguez and Gennaro (2014), only the main results are exposed here. The central manifold expansion of the flowfield is found to be of the form

$$\mathbf{q} = \bar{\mathbf{q}} + (A\hat{q}\mathrm{e}^{\mathrm{i}\beta_c z} + c.c.) + \hat{\delta}A\mathbf{q}_{11} + |A|^2\mathbf{q}_{20} + (A^2\mathbf{q}_{22}\mathrm{e}^{\mathrm{i}2\beta_c z} + c.c.) + \dots, \qquad (1)$$

where A is the bifurcation or disturbance amplitude, $\hat{\delta}$ is a measure of the deviation from the critical conditions and the two-dimensional shape-functions $\mathbf{q}_{11}$, $\mathbf{q}_{20}$ and $\mathbf{q}_{22}$ describe flowfield modifications originated by nonlinear interactions.

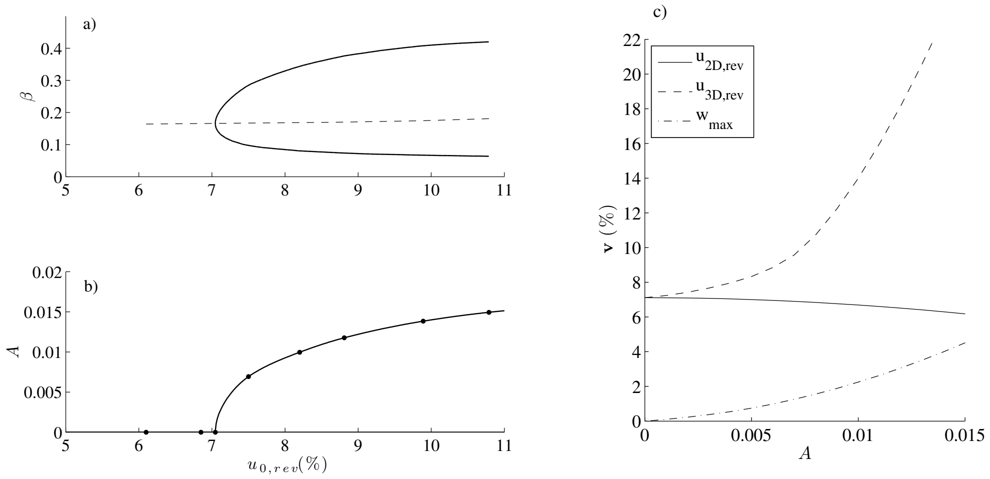

Figure 2. (a) Neutral instability curve of the primary global eigenmode; spanwise wavenumber β against peak recirculation in the base flow, $u_{0,\mathrm{rev}}$. The dashed line shows the least stable/most unstable wavenumber for each recirculation. (b) Bifurcation diagram corresponding to the primary instability: saturated disturbance amplitude A against $u_{0,\mathrm{rev}}$ (negative values of A are not shown). (c) Peak reversed flow and spanwise velocities of the bifurcated flow, as a function of the amplitude A. Thick line: peak reversed velocity of the spanwise-mean bifurcated flow; dashed line: peak reversed velocity of the bifurcated flow; dashed-dotted: peak spanwise velocity. All velocities are shown as percentage of the far-field velocity at inflow.

In a similar manner, a Landau equation for the time-evolution of A is obtained as a expansion in terms of the bifurcation parameters A and $\hat{\delta}$:

$$\mathrm{dA/dt} = \mathrm{h_{11}}\hat{\delta}\mathrm{A} + \mathrm{h_{31}}|\mathrm{A}|^2\mathrm{A}, \tag{2}$$

where h_{11} and h_{31} being two constants also determined by the WNL expansion. In particular, it is found that $h_{11}\hat{\delta} \approx \omega_i(\hat{\delta})$, i.e. the linear growth rate of the leading mode for a perturbed $\bar{\mathbf{q}}$ close to the critical conditions. A value $h_{31} = -3.26$ is found from the cancellation of secular terms in the WNL expansion, dictating that the primary bifurcation is a supercritical pitchfork one. Landau equation (2) and central manifold (1) describe the following evolution for slightly unstable conditions ($\omega_i > 0$): First, the amplitude A grows exponentially in time due to the linear instability. As A grows, nonlinear interactions generate a modification of the spanwise-homogeneous (2D) component of the flow ($|A|^2\mathbf{q}_{20}$), as well as the appearance of flow components associated with harmonics of the fundamental spanwise wavenumber ($A^2\mathbf{q}_{22}\mathrm{e}^{\mathrm{i}2\beta_c x}$+$c.c.$). Higher harmonics will also appear, but they will be $O(A^5)$ at most. Nonlinear interactions will gradually redistribute the energy that is extracted from the base separation bubble by the centrifugal instability, and the amplitude growth saturate at an amplitude given by setting $\mathrm{dA/dt} = 0$ in (2). The relation between equilibrium A and $\bar{\delta}_{max}$ or $u_{0,rev}$ (as proxies to $\hat{\delta}$) defines the bifurcation diagram, shown in figure 2 (b).

The bifurcation associated with the primary instability describes how the initially steady and two-dimensional base separation bubble transitions to a steady three-dimensional separation bubble, in the absence of external disturbances or forcing. Due to the structurally unstable nature of two-dimensional topologies, three-dimensionalization will originate qualitatively different separation bubbles even for very low bifurcation amplitudes A. To illustrate these differences, two bifurcated flows are considered in what follows:

$$\bar{\mathbf{q}}_{3D} = \bar{\mathbf{q}} + (A\hat{\mathbf{q}}\mathrm{e}^{\mathrm{i}\beta_c z} + c.c.) + |A|^2\mathbf{q}_{20} + (A^2\mathbf{q}_{22}\mathrm{e}^{\mathrm{i}2\beta_c z} + c.c.), \quad \text{and} \tag{3}$$

$$\bar{\mathbf{q}}_{2D} = \bar{\mathbf{q}} + |A|^2\mathbf{q}_{20}. \tag{4}$$

The first flow, $\bar{\mathbf{q}}_{3D}$, is the three-dimensional bifurcated flow obtained from the expansion (1), where $\delta h A\mathbf{q}_{11}$ has been neglected due to its small amplitude. The second flow, $\bar{\mathbf{q}}_{2D}$ only comprises the spanwise-homogeneous flowfield, being equivalent to a spanwise averaged flow. Figure 2(c) shows the changes in the peak reversed flow and spanwise velocity component as a function of the bifurcation amplitude for $\bar{\mathbf{q}}_{2D}$ and $\bar{\mathbf{q}}_{3D}$. The three-dimensionalization of the flow also increases the reversed flow at certain spanwise planes, so that maximum recirculations larger than those of the base separation bubble are attained. On the other hand, the changes in the peak reversed flow in the two-dimensional bifurcated flow are comparatively much weaker. As will be shown later, the two bifurcated flows have very different secondary instability properties.

Figure 3 summarizes the flow bifurcation occurring as a consequence of the primary, centrifugal instability. Figure 3(a) shows the two-dimensional laminar separation bubble model, constructed as explained in section 2.1 This two-

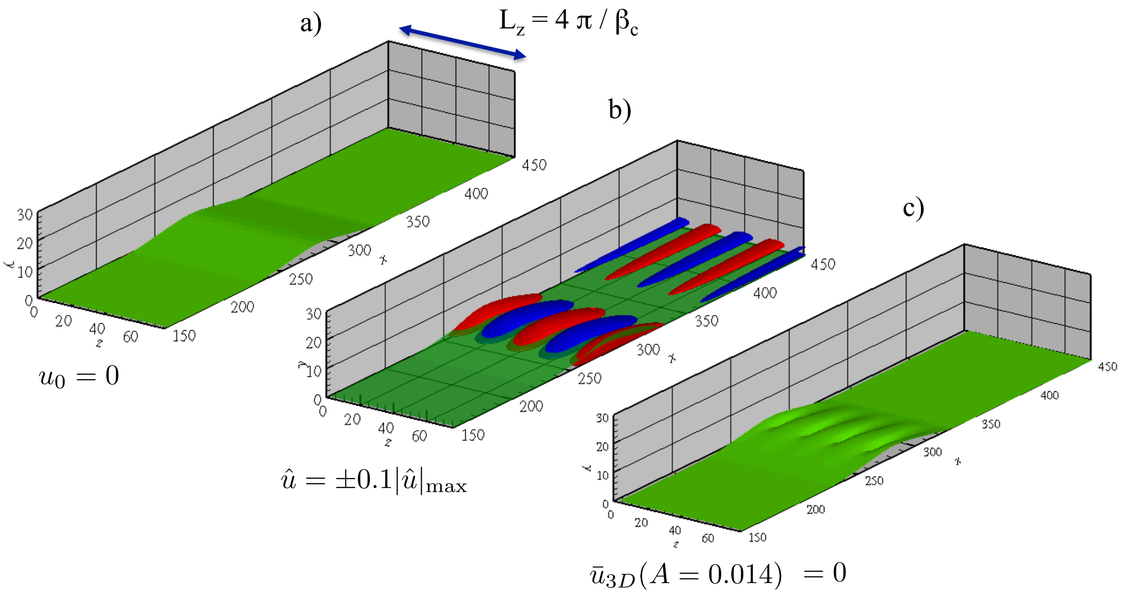

Figure 3. Three-dimensional visualizations of the laminar separation bubble. (a) $\bar{u}_0 = 0$ iso-surface for the base two-dimensional separation bubble. (b) The green iso-surface is the same as in (a), red and blue iso-surfaces show the streamwise velocity perturbation corresponding to the primary instability eigenmode. (c) $\bar{u}_{3D} = 0$ iso-surface for the three-dimensional flow, obtained by the WNL expansion, at the saturation amplitude $A = 0.014$. Two spanwise periods of the dominant primary instability eigenmode are shown.

dimensional flow is unstable with respect a three-dimensional (spanwise-periodic) eigenmode, shown in figure 3(b). This instability, in the absence of any imposed external disturbance or forcing term, leads to a three-dimensionalization of the flow. A bifurcated flowfield appears as the amplitude associated with the three-dimensional eigenmode increases, and nonlinear interactions between the eigenmode and the base flow give rise to a modification of the latter, as well to the appearance of perturbation components on spanwise wavenumber that are harmonics of that of the primary eigenmode. Finally, saturation of the disturbance growth happens and a steady, fully three-dimensional separation bubble is reached (figure 3(c)).

3. SECONDARY INSTABILITY ANALYSIS OF THREE-DIMENSIONAL SEPARATION BUBBLES

The primary instability analyses of the base two-dimensional laminar separation bubbles showed that there is not an instability that would give rise to self-excited oscillations of the flow field, in the absence of a external forcing or source of disturbances. The bifurcated two- and three-dimensional laminar separation bubble flows discussed in the previous section, that appear as a consequence of the centrifugal instability, are steady. The question arises whether these bifurcated flowfields support a secondary instability that originates unsteadiness. This question is addressed now by means of a linear, secondary instability analysis of the bifurcated flowfields.

The three-dimensionality of flowfield $\bar{\mathbf{q}}_{3D}$ implies that simplifications of common use in the literature for the instability analysis, like neglecting the influence of spanwise variations of the base flow, cannot be done. In principle, a modal instability analysis of a three-dimensional flow $\bar{\mathbf{q}}(x, y, z)$ would require the computation of eigenmodes $\hat{\mathbf{q}}(x, y, z)\exp(-\mathrm{i}\omega t)$, that depend in a inhomogeneous manner on the three spatial directions. The spatial discretization of this three-dimensional eigenmode stability analysis (sometimes referred to as tri-global) results into very large matrices.

A different methodology is proposed here, based on the assumption that the flowfields under consideration are only slowly-varying along the streamwise direction. This is generally true in boundary-layer flows, but the existence of a closed region of recirculating fluid may involve streamwise variations of the fluid variables comparable to the cross-sectional variables; the validity of the assumption for a particular flow can only be checked *a posteriori*. Under this weakly non-parallel approximation, we can derive a series of two-dimensional eigenvalue problems for the *local* stability of the cross-sectional velocity profiles. The existence of globally synchronized oscillations along the streamwise direction is then studied based on the absolute or convective character of the instability waves at the successive streamwise locations. This method, and extension of the *global* approach by Huerre and Monkewitz (1990); Chomaz *et al.* (1991) to three-dimensional flows, enables the study of instabilities giving rise to self-excited global oscillations at a small fraction of the cost of performing a three-dimensional eigenmode analysis.

3.1 METHODOLOGY

Assuming that the flowfield $\bar{\mathbf{q}}(x,y,z)$ is slowly dependent on the streamwise direction x, i.e. $\partial\bar{\mathbf{q}}/\partial x \ll \partial\bar{\mathbf{q}}/\partial y, \partial\bar{\mathbf{q}}/\partial z$, we can introduce a separation in scales by defining the new *long* coordinate $X = \epsilon x$ with $\epsilon \ll 1$. Then, the perturbations can be written as

$$\mathbf{q}' \sim \hat{\mathbf{q}}(y,z;X)\exp\left[\mathrm{i}(\alpha(X)x - \omega t)\right] + c.c. \tag{5}$$

In this expression, the long coordinate X only enters as a parameter on the shape functions $\hat{\mathbf{q}}$ and in the streamwise wavenumber α. Substituting this decomposition into the linearized Navier-Stokes equations, we arrive at a series of eigenvalue problems for the local instability of cross-sectional velocity profiles:

$$\mathcal{L}(\bar{\mathbf{q}}(y,z;X),\alpha)\hat{\mathbf{q}} = -\mathrm{i}\omega\mathcal{R}\hat{\mathbf{q}}. \tag{6}$$

Linear operator $\mathcal{L}$ depends solely on velocity field at the cross-plane X, and the eigenfunctions $\hat{\mathbf{q}}$ are two-dimensional. Through the solution of the eigenvalue problem problem (6), a dispersion relation is constructed that describes the local behavior of instability waves:

$$\mathcal{D}(\alpha,\omega,X) = 0, \qquad \text{with } \alpha,\omega \in \mathbb{C}. \tag{7}$$

The analysis proceeds by studying the absolute or convective nature of the instability waves at each streamwise location. Absolutely unstable waves are those that grow in amplitude while they propagate upstream from their introduction point; convectively unstable waves are those that grow in amplitude while being convected downstream, but decrease in amplitude for an observer fixed at the introduction point. This behavior is determined by the absolute frequency $\omega_0(X)$, defined as the complex frequency corresponding to the waves with zero group velocity:

$$\omega_0(X) = \left\{\omega \in \mathbb{C} \Big/ v_g = \frac{\partial\omega}{\partial\alpha}(\omega_0, X) = 0\right\}. \tag{8}$$

The imaginary part of the absolute frequency, $\omega_{0,i}$ determines if temporal growth exists for waves in the ray $x/t = 0$. If $\omega_{0,i} > 0$, a perturbation imposed at a certain $X-$location will grow in amplitude in that same location and the flow is absolutely unstable at that location. If $\omega_{0,i} < 0$, the perturbation at X will decrease in time, and then the perturbation waves can be convectively unstable if their amplitude grows as they propagate downstream, or stable if the amplitude decays everywhere. The saddle-point condition also implies that the global frequency is the point on the complex $\omega-$planes where two solution branches of α, α^+ and α^-, pinch.

Globally synchronized oscillations may exist if the base flow $\bar{\mathbf{q}}$ is absolutely unstable over a streamwise region of large enough spatial support; then a feed-back mechanism between instability waves propagating upstream and downstream gives rise to self-sustained oscillations. The complex frequency of such oscillator, referred to as global frequency ω_g, is given by the saddle point of ω_0 on the complex $X-$plane (Huerre and Monkewitz (1990); Chomaz *et al.* (1991)). The complex $X-$coordinate where the saddle-point condition is verified is known as the wavemaker X_s, as it is the spatial location where the feed-back produces the dominant global oscillations:

$$X_s = \left\{X \in \mathbb{C} \Big/ \frac{\partial\omega_0}{\partial X}(X_s) = 0\right\}. \tag{9}$$

The global oscillator frequency is then defined as $\omega_g = \omega_0(X_s)$, and it is in general a complex quantity. If $\omega_{g,i} > 0$ the amplitude of the global oscillations will grow exponentially with time, until nonlinear effects set in, and the flow $\bar{\mathbf{q}}$ under consideration will be unstable. Otherwise, if $\omega_{g,i} < 0$, the global oscillations are temporally damped, and the bifurcated flows will remain steady.

Once the global oscillation frequency is determined, the spatial shape of the perturbations can be recovered from the WKB approximation:

$$\mathbf{q}'(x,y,z,t) = A(X)\hat{\mathbf{q}}^{\pm}(y,z;X)\exp\left(\mathrm{i}\int_0^x \alpha^{\pm}(X')dx' - \mathrm{i}\omega_g t\right) + c.c. \tag{10}$$

In first-order approximation, $A(X)$ can be taken to be a constant (Juniper *et al.* (2011)). $\hat{q}^{\pm}$ and $\alpha^{\pm}$ correspond respectively to the eigenfunctions and wavenumbers corresponding to the continuous branches of the local instability eigenmodes upstream and downstream of the wavemaker location.

The most straight-forward alternative to this elaborated methodology is the computation of three-dimensional eigenmodes. In this case, the only assumption is that the base flow $\bar{\mathbf{q}}$ is time-independent, and following from its dimensionality we arrive at the eigenvalue problem

$$\mathcal{L}(\bar{\mathbf{q}}(x,y,z))\hat{\mathbf{q}} = -\mathrm{i}\omega\mathcal{R}\hat{\mathbf{q}}, \tag{11}$$

where now the eigenfunctions $\hat{\mathbf{q}}(x,y,z)$ and linear operators $\mathcal{L}$ and $\mathcal{R}$ depend in a coupled manner of the three spatial directions. While the formulation is much simpler, the numerical resolution of this *tri-global* eigenvalue problem is more expensive than the proposed WKB approach by an order of magnitude in memory and computational time.

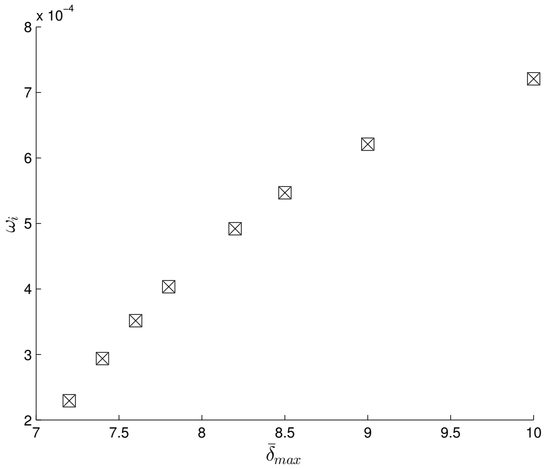

Figure 4. Comparison of the linear growth rate of the leading mode obtained between the global stability analyses (squares) and the direct numerical simulations (DNS) (times symbols).

3.2 NUMERICAL METHODS AND IMPLEMENTATION

For the computations presented herein, we employed a novel stability code based on Gennaro (2012) and Gennaro *et al.* (2013). Sixth-order standard finite differences are used for the discretization of the two-dimensional and three-dimensional linear operators $\mathcal{L}$ and $\mathcal{R}$ defining the stability eigenvalue problems (6, 11). Analytical transformations are used to cluster grid points in regions of large gradients.

After discretization, the eigenvalue problems are solved using an in-house implementation of the shift-and-invert Arnoldi algorithm. This Krylov's subspace iteration allows for the efficient computation of an arbitrarily large window of the eigenspectrum at a small fraction of the cost of alternatives like the QZ algorithm. Matrix operators are formed and operated on in sparse format. In-house routines are used for matrix-vector and matrix-matrix operations, while the ordering library METIS and the multifrontal solver library MUMPS (Amestoy *et al.* (2001)) are used for the computation of LU decompositions and back-substitutions. The use of sparse storage and operations reduces drastically the computational resources required for the solution as compared to an equivalent dense-algebra computation.

Most of the results presented below were obtained in a laptop computer featuring 4 Gbytes of Memory. The largest two-dimensional eigenvalue problems (6) considered for validation used a resolution $N_x \times N_y = 201 \times 121$, and required around 10 minutes for the computation of the leading 500 eigenmodes. However, in the computation of the three-dimensional oscillator by means of the weakly non-parallel approach, a resolution of only $N_y \times N_z = 81 \times 41$ was required for a reasonable convergence of the results; the solution of each one of these problems took less than one minute.

Three-dimensional eigenvalue problems of the class of (11) were solved in a shared-memory machine with access to 128 Gbytes of memory. The largest computation performed here, with a resolution of $N_x \times N_y \times N_z = 221 \times 51 \times 21$ points, employed slightly less than 10 hours to compute the leading 2000 eigenmodes.

Perfect agreement between the predictions of the linear growth rate of the leading mode obtained by means the global stability analyses, denoted by square symbols in the figure (4), and the direct numerical simulations is attained. For the direct numerical simulations a numerical code for the Navier-Stokes equations written in velocity-vorticity formulation for three-dimensional, incompressible flow was used. The method uses high-order finite-difference schemes in streamwise and wall normal directions and spectral approximations in the spanwise direction. The time integration is carried out by a 4th order Runge-Kutta scheme. Details of the adopted method can be seen in Petri *et al.* (2015) and Malatesta *et al.* (2015).

3.3 RESULTS

The weakly non-parallel methodology for the linear stability analysis of three-dimensional flows in which the gradient of the flow properties along the streamwise direction is weak compared with that on the cross-sections is used in this section to analyze the secondary instability of the laminar separation bubbles. The steady laminar separation bubbles recovered by the weakly nonlinear expansion discussed in section (2.3) are considered now as base flows. The two bifurcated flows, $\bar{\mathbf{q}}_{2D}$ and $\bar{\mathbf{q}}_{3D}$, are analyzed in order to clarify the impact of three-dimensionality on the instability of the flow.

Figure 5 shows the evolution of the complex global frequency ω_g and wavemaker location X_s corresponding to the dominant global oscillator found, as a functions of the bifurcation amplitude A. In line with the analyses for the initial base flow $\mathbf{q}_0$ presented in Rodríguez *et al.* (2013), the imaginary part of the global frequency ω_g is negative for low values of A, implying a temporal decay of the global oscillation mode. The results for the $\bar{\mathbf{q}}_{2D}$ and $\bar{\mathbf{q}}_{3D}$ flows are very

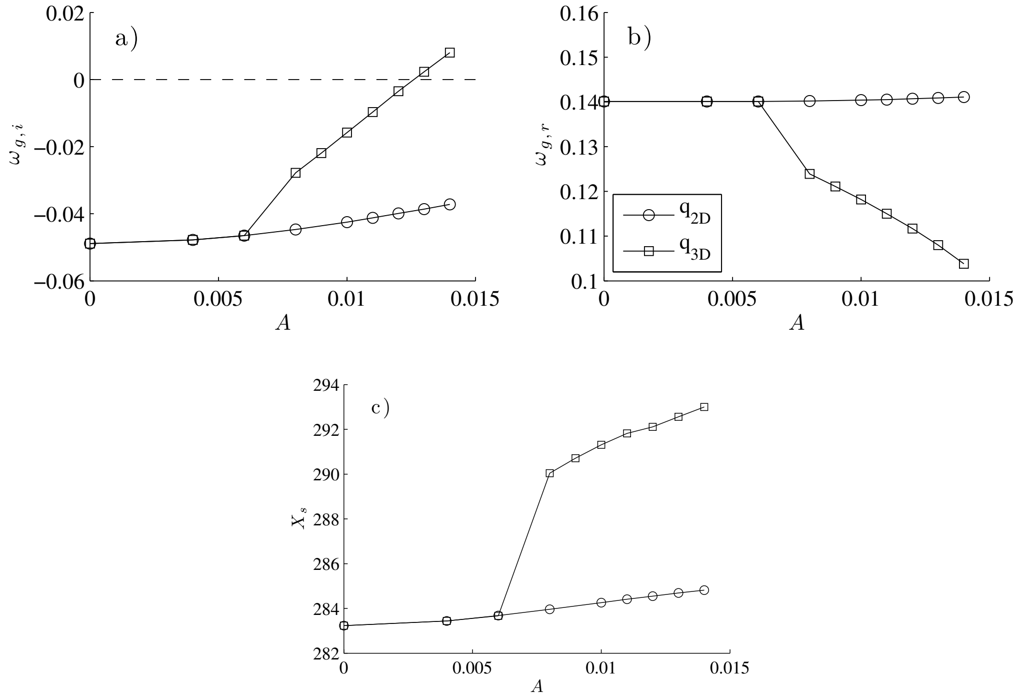

Figure 5. Imaginary (a) and real (b) components of the global oscillator frequency, and real wavemaker location X_s, computed for spanwise-averaged and 3D bifurcated flows $\bar{\mathbf{q}}_{2D}$ (circles) and $\bar{\mathbf{q}}_{3D}$ (squares).

similar up to some amplitude between $A = 0.006$ and $A = 0.008$. Substantial differences appear between the global frequency and wavemaker location for the spanwise-averaged and 3D flows as A is increased further: the imaginary part of ω_g approaches zero rapidly and the oscillation frequency decreases for $\bar{\mathbf{q}}_{3D}$, while very small variations are observed for $\bar{\mathbf{q}}_{2D}$. In addition, the wavemaker for $\bar{\mathbf{q}}_{3D}$ is markedly displaced downstream, from the approximate $x-$coordinate corresponding to the largest displacement thickness in the spanwise-averaged flow towards the location where the peak spanwise velocity is attained. This difference in the global oscillator characteristics between spanwise-averaged and 3D flows is motivated by a change in the dominant eigenmode found in the *local* cross-stream sections for $A > 0.006$: the spanwise velocity gradients in the 3D-bifurcated flow give rise to additional inflectional instabilities, the effect of which become dominant at this amplitude. A refined analysis would be required to determine accurately the amplitude at which the change in the dominant local eigenmode happens.

For $A > 0.0127$, the 3D global mode becomes temporally amplified and a self-excited global oscillator exists. At the critical conditions, $A \approx 0.0127$, the peak reversed flow and spanwise velocity attained in some spanwise locations within the 3D steady bubble exceeds respectively 18% and 3% of the free-stream velocity. Note that the value of $u_{3D,rev} = 18\%$ for the global instability is in line with the $u_{rev} = 15\%$ threshold given in the literature for absolute instability in 2D wall-bounded separated profiles.

Figure 6(a) shows the streamwise velocity field $\hat{u}$ corresponding to the global oscillator for $A = 0.014$, characterized by $\omega_g = 0.1039 + \mathrm{i}0.0078$. The unsteady velocity field is computed downstream of the wavemaker by applying equation (10). The cross-sectional plane closest to the wavemaker X_s is also shown, along with the streamwise velocity contours. Fluctuations associated with the secondary instability are highly localized; the peak fluctuations at the wavemaker plane appear on those spanwise locations where the peak reversed flow is higher, and extend sideways in the regions where the strongest spanwise velocity gradients in $\bar{\mathbf{q}}_{3D}$ exist. These fluctuations propagate downstream while growing in amplitude until approximately the reattachment location of separated shear layer, where the peak disturbance velocities are attained, and are gradually damped afterwards. It should be noted this global oscillator mode is linear: temporal amplification of these fluctuations will eventually give rise to new nonlinear interactions that will distort their spatial structure in a manner which is not predicted in the present computations and that can differ remarkably from figure 6(a).

In order to validate the results obtained by the weakly non-parallel methodology, a three-dimensional eigenmode analysis (11) for the same base flow ($\bar{\mathbf{q}}_{3D}$) is done. The most unstable mode found amongst the leading 2000 eigenmodes corresponds to the complex frequency $\omega = 0.105 + \mathrm{i}0.0075$, and its corresponding streamwise velocity field is shown in figure 6(b). The excellent visual comparison between the eigenfunctions and the relative mall difference between the complex frequencies, below 1%, indicates that the two methodologies recovered accurately the same secondary instability.

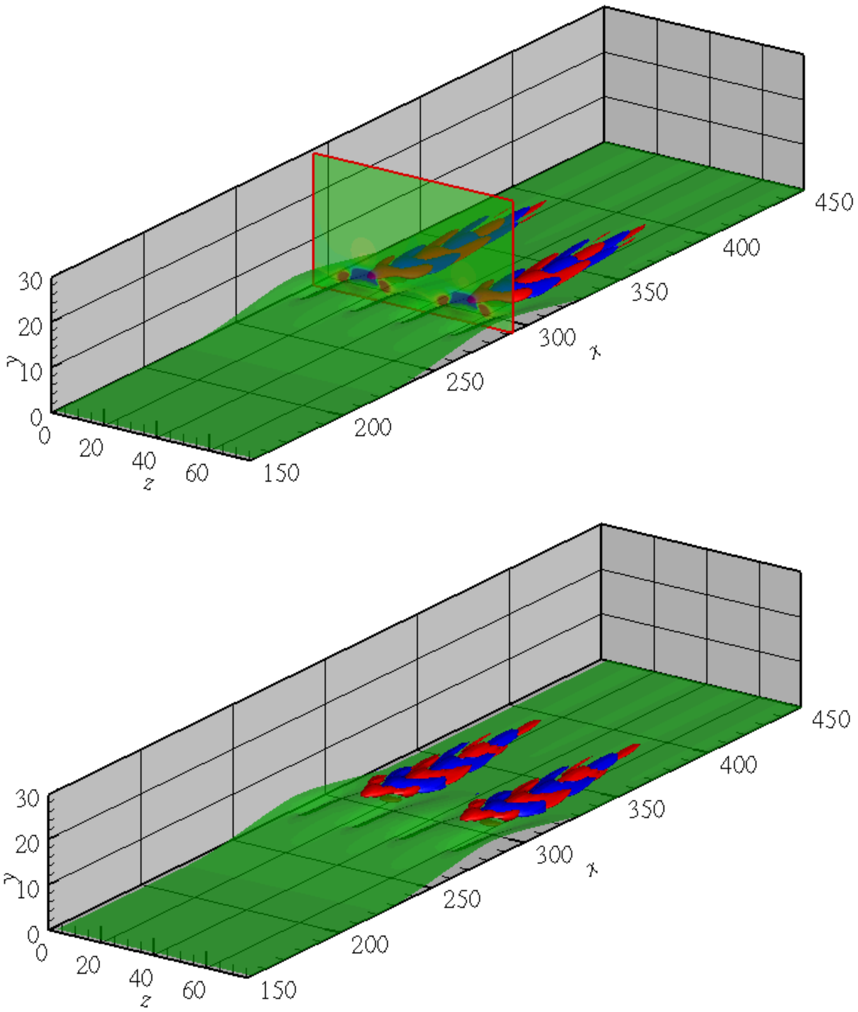

Figure 6. Streamwise perturbations corresponding to 3D global modes of the bifurcated flow $\bar{\mathbf{q}}_{3D}$ at $A = 0.014$. Left: Global oscillator obtained by WKB method on cross-planes ($\omega_g = 0.1039 + \mathrm{i}0.0078$). Right: Leading three-dimensional eigenmode ($\omega = 0.108 + \mathrm{i}0.0075$). Green: $\bar{u}_{3D} = 0$. Blue/red: $\hat{u} = \pm 0.1|\hat{u}|_{\max}$.

4. SUMMARY AND CONCLUSIONS

Laminar separation bubbles sustain an intrinsic three-dimensional instability which dominates the flow physics in the absence of external forcing. A weakly nonlinear analysis shows that it corresponds to a supercritical pitchfork bifurcation that breaks the spanwise homogeneity of the base two-dimensional bubbles generating spanwise gradients that modify the instability properties of the resulting three-dimensional bubble.

Secondary instability analyses of the steady three-dimensional laminar separation bubbles that appear as a consequence of the primary flow bifurcation are done in this paper. A novel methodology is proposed for this analysis, which extends the weakly non-parallel analysis of Huerre and Monkewitz (1990) and Chomaz *et al.* (1991) to three-dimensional flows. The results for the secondary stability analysis are cross-validated with those of a three-dimensional eigenmode analysis. Both approaches recover independently the same global oscillator, but the computational cost associated with the latter is at least one of magnitude higher: the weakly non-parallel analysis is based on two-dimensional eigenvalue problems for cross-sections and can be solved on a laptop, while the validation three-dimensional eigenmode analysis required of a shared-memory machine featuring 128 Gbytes.

Present results show that the three-dimensional separation bubbles originated by the primary, centrifugal instability can sustain a self-excited secondary instability that originates flow oscillations in an otherwise steady flow. The peak reversed flow attained within the separation bubble at the critical conditions of the secondary instability is found to be $u_{rev,3D} \approx 18\%$, in agreement with results in the literature for the absolute instability for two-dimensional separation bubbles (Alam and Sandham (2000); Rist and Maucher (2002)). On the other hand, the spatial structure of the associated velocity fluctuations suggests that this mode can be related to the origin of the transitional structures observed in the literature (Alam and Sandham (2000); Watmuff (1999)). Another question that is addressed in this paper is the relevance of the analysis of a spanwise-averaged separation bubbles in the study of the instability of unforced separation bubbles. This assumption is commonly done in order to characterize the spatial amplification of time periodic disturbances introduced upstream of the separation, and has been shown to deliver good comparisons with experiments and simulations (e.g. Dovgal *et al.* (1994)). This can be explained by the very large spatial amplification rates of the inflectional instability due to the separated shear layer, that results in important amplifications of the forced disturbances. However, this inflection instability is of convective nature and in the absence of continuous forcing the fluctuations would be advected downstream eventually leaving the separation bubble unaffected. The analyses presented herein show that, for *unforced* separation bubbles in which the amplifier behavior of separation bubbles cannot be manifested, considering a spanwise-averaged base flow in the secondary instability study does not recover the global oscillator. The three-dimensionality of the separation bubble originated by the primary instability is concluded to play a fundamental role in the origin of self-sustained unsteadiness of laminar separation bubbles in the absence of external excitations.

Finally, it should be remarked that present study considers only linear or weakly nonlinear methods. A fully non-linear study is necessary in order to verify these results and complete the understanding of the physical picture put forward here.

5. ACKNOWLEDGEMENTS

The work of D.R. is funded by the Science without borders/CAPES- "Attraction of Young Talents" Fellowship. This work is supported by São Paulo Research Foundation (FAPESP) grants 2014/24782-0.

6. REFERENCES

Alam, M. and Sandham, N.D., 2000. "Direct numerical simulation of 'short' laminar separation bubbles with turbulent reattachment". *J. Fluid Mech.*, Vol. 410, pp. 1–28.

Allen, T. and Riley, N., 1995. "Absolute and convective instabilities in separation bubbles". *Aeronautical Journal*, Vol. 99, pp. 439–448.

Amestoy, P.R., Duff, I.S., L'Excellent, J.Y. and Koster, J., 2001. "A fully asynchronous multifrontal solver using distributed dynamic scheduling". *SIAM J. Matrix Anal. Appl.*, Vol. 23, No. 1, pp. 15–41. ISSN 0895-4798.

Carter, J., 1975. "Inverse solutions for laminar boundary-layer flows with separation and reattachment". Technical Report NASA TR R-447.

Chomaz, J.M., Huerre, P. and Redekopp, L., 1991. "A frequency selection criterion in spatially-developing flows". *Stud. Appl. Maths*, Vol. 84, pp. 119–144.

Dallmann, U. and Schewe, G., 1987. "On topological changes of separating flow structures at transition reynolds numbers". AIAA, Honolulu, HI, number Paper 87-1266 in 16th Fluid Dynamics, Plasma Dynamics and Lasers Conference.

Dovgal, A., Kozlov, V. and Michalke, A., 1994. "Laminar boundary layer separation: instability and associated phenomena". *Prog. Aero. Sci.*, Vol. 3, pp. 61–94.

Gennaro, E.M., 2012. *Análise da estabilidade global de escoamentos compressíveis*. Ph.D. thesis, Universidade de São Paulo.

Gennaro, E.M., Rodríguez, D., Medeiros, M.A.F. and Theofilis, V., 2013. "Sparse techniques in global flow instability with application to compressible leading-edge flow". *AIAA J.*, Vol. 51, No. 9, pp. 2295–2303.

Hammond, D. and Redekopp, L., 1998. "Local and global instability properties of separation bubbles". *Eur. J. Mech. B/Fluids*, Vol. 17, pp. 145–164.

Horton, H., 1969. "A semi-empirical theory for the growth and bursting of laminar separation bubbles". *ARC CP*, Vol. 1073.

Huerre, P. and Monkewitz, P., 1990. "Local and global instabilities in spatially developing flows". *Ann. Rev. of Fluid Mechanics*, Vol. 22, pp. 473–537.

Juniper, M.P., Tammisola, O. and Lundell, F., 2011. "The local and global stability of confined planar wakes at intermediate reynolds number". *J. Fluid Mech.*, Vol. 686, pp. 218–238.

Malatesta, V., Souza, L.F., Liu, J.T. and Kloker, M.J., 2015. "Heat transfer analysis in a flow over concave wall with primary and secondary instabilities". *Procedia IUTAM*, Vol. 14, pp. 487 – 495. IUTAM-ABCM Symposium on Laminar Turbulent Transition.

Petri, L.A., Sartori, P., Rogenski, J.K. and de Souza, L.F., 2015. "Verification and validation of a direct numerical simulation code". *Computer Methods in Applied Mechanics and Engineering*, Vol. 291, pp. 266 – 279.

Rist, U. and Maucher, U., 2002. "Investigations of time-growing instabilities in laminar separation bubbles". *Eur. J. Mech. B/Fluids*, Vol. 21, pp. 495–509.

Rodríguez, D., 2010. *Global stability of laminar separation bubbles*. Ph.D. thesis, Universidad Politécnica de Madrid.

Rodríguez, D. and Gennaro, E.M., 2014. "On the secondary instability of forced and unforced laminar separation blubbles". *Procedia IUTAM*, Vol. 14, pp. 78 – 87. IUTAM-ABCM Symposium on Laminar Turbulent Transition, Rio de Janeiro, Brazil.

Rodríguez, D., Gennaro, E.M. and Juniper, M.P., 2013. "The two classes of primary modal instability in laminar separation bubbles". *J. Fluid Mech.*, Vol. 734, p. R4.

Rodríguez, D. and Theofilis, V., 2010. "Structural changes of laminar separation bubbles induced by global linear instability". *J. Fluid Mech.*, Vol. 655, pp. 280–305.

Theofilis, V., Hein, S. and Dallmann, U., 2000. "On the origins of unsteadiness and three-dimensionality in a laminar separation bubble." *Phil. Trans. Roy. Soc. London (A)*, Vol. 358, pp. 3229–3246.

Watmuff, J.H., 1999. "Evolution of a wave packet into vortex loops in a laminar separation bubble". *J. Fluid Mech.*, Vol. 397, pp. 119–169.

7. RESPONSIBILITY NOTICE

The authors are the only responsible for the printed material included in this paper.